

Article

Channel Bed Adjustment of the Lowermost Yangtze River Estuary from 1983 to 2018: Causes and Implications

Ming Tang^{1,2,3} , Heqin Cheng^{2,4,*} , Yijun Xu^{3,5,*} , Hao Hu⁶, Shuwei Zheng⁷, Bo Wang⁸ , Zhongyong Yang⁹, Lizhi Teng², Wei Xu², Erfeng Zhang² and Jiufa Li²

- ¹ School of Computer Engineering and Science, Shanghai University, Shanghai 200444, China
² State Key Lab of Estuarine & Coastal Research, East China Normal University, Shanghai 200241, China
³ School of Renewable Natural Resources, Louisiana State University Agricultural Center, Baton Rouge, LA 70803, USA
⁴ Institute of Eco-Chongming, East China Normal University, Shanghai 200241, China
⁵ Coastal Studies Institute, Louisiana State University, Baton Rouge, LA 70803, USA
⁶ School of Urban and Planning, Yancheng Teachers University, Yancheng 224002, China
⁷ College of Geography and Environment, Shandong Normal University, Jinan 250358, China
⁸ Institute at Brown for Environment and Society, Brown University, Providence, RI 02912, USA
⁹ College of Hydraulic and Environment Engineering, China Three Gorges University, Yichang 443002, China
* Correspondence: hqch@sklec.ecnu.edu.cn (H.C.); yjxu@lsu.edu (Y.X.)



Citation: Tang, M.; Cheng, H.; Xu, Y.; Hu, H.; Zheng, S.; Wang, B.; Yang, Z.; Teng, L.; Xu, W.; Zhang, E.; et al. Channel Bed Adjustment of the Lowermost Yangtze River Estuary from 1983 to 2018: Causes and Implications. *Water* **2022**, *14*, 4135. <https://doi.org/10.3390/w14244135>

Academic Editor: Giuseppe Oliveto

Received: 15 November 2022

Accepted: 13 December 2022

Published: 19 December 2022

Publisher's Note: MDPI stays neutral with regard to jurisdictional claims in published maps and institutional affiliations.



Copyright: © 2022 by the authors. Licensee MDPI, Basel, Switzerland. This article is an open access article distributed under the terms and conditions of the Creative Commons Attribution (CC BY) license (<https://creativecommons.org/licenses/by/4.0/>).

Abstract: Deltaic channels are significant landforms at the interface of sediment transfer from land to oceanic realms. Understanding the dynamics of these channels is urgent because delta processes are sensitive to climate change and adjustments in human activity. To obtain a better understanding of the morphological processes of large deltaic channels, this study assessed the evolution and response mechanism of the South Channel and South Passage (SCSP) in the Yangtze Estuary between 1983 to 2018 using hydrology, multibeam echo sounding and historical bathymetry datasets. Decadal changes in riverbed volume and erosion/deposition patterns in the SCSP were assessed. The results showed that the SCSP experienced substantial deposition with a total volume of $26.90 \times 10^7 \text{ m}^3$ during 1983–2002, but significant bed erosion with a total volume of $26.04 \times 10^7 \text{ m}^3$ during 2003–2010. From 2011 to 2018, the estuarine riverbeds shifted from erosive to depositional, even though the deposition was relatively marginal ($0.76 \times 10^7 \text{ m}^3$). We inferred that the SCSP have most likely changed from a net erosion phase to a deposition stage in response to local human activities including sand mining, river regulation project, and Deep Water Channel Regulation Project). The channel aggradation will possibly continue considering sea level rise and the ongoing anthropogenic impacts. This is the first field evidence reporting that the lowermost Yangtze River is reaching an equilibrium state in terms of channel erosion and, in fact, the Yangtze River Estuary channels are beginning to aggrade. The findings have relevant implications for the management of the Yangtze River and other lowland alluvial rivers in the world as global sea level continues rising and human intervention on estuarine systems persists.

Keywords: channel dynamics; sediment transport; microtopography; anthropogenic stresses; deltaic channel; Yangtze River

1. Introduction

Suspended sediment loads in many rivers in the world have declined sharply in the past century due primarily to dam construction, river engineering, and soil conservation practices [1–3]. A reduction in riverine sediment can lead to an increase in the river's sediment-carrying capacity, which will cause river channels to adjust to the new flow-sediment conditions. Several studies reported channel adjustment following river engineering, e.g., channel erosion in the lower Yangtze River after the Three Gorge Dam (TGD) construction [4] and in the upper Atchafalaya River after a Mississippi River diversion

control was built [4,5]. The channel erosion resulted in substantial riverbed downcutting and large quantities of bed material moving downstream in these alluvial rivers. Collectively, these studies have increased our knowledge on river channel dynamics in response to human activities. However, less is known about how river reaches in their deltaic areas respond to the upstream adjustment to the sediment load reduction.

Deltaic channels present the final link of terrestrial sediment transport into the oceans, playing a significant role in coastal systems [6,7]. The geomorphic evolution of deltaic channels is of great significance in terms of infrastructure safety, navigation maintenance, and ecological service function. However, most of the world's river deltas are at risk of sea levels rising and land subsidence [8]. Thus, the geomorphological dynamics and behavior of deltaic channels in response to dramatic climatic and anthropogenic stresses are receiving increased attention [9–14]. For example, sediment trapping in the Mississippi River basin has led to severe inundation of the delta plain and the loss of marsh habitat [15,16]. However, the Yellow River delta [17] and the Pearl River delta [18] in China converted to net erosion at the subaqueous deltas due to insufficient sediment supply and human activities. To maintain the erosion–deposition balance in the delta, a certain amount of fluvial sediment transport is required [19], and it has been reported that a portion of this supply is increasingly sourced by scouring from the upstream channel, given severe decreases in sediment caused by river damming [5,20]. Hence, some case studies of deltaic channels with the latest data are required to better understand the processes of geomorphic evolution under fluvial sediment decline and anthropogenic interferences.

Similar to other large rivers, the Yangtze River, the third longest river in the world, has been remarkably affected in its sediment transport and channel dynamics by upstream dam constructions, especially the Three Gorges Dam. Yang et al. [21] postulated that the 50,000 dams built in the Yangtze River Basin have caused significant erosion of the river's subaqueous delta. While a recent study showed that erosion only occurred locally and there is no obvious trend of erosion within the Yangtze River Delta (YRD), even with a sharp decline in sediment load [22]. Consequently, there is no consistent conclusion on the evolution of the deltaic channel in response to engineering interferences. A study by Xie and others [23] predicted the morphodynamic evolution of the Yangtze River Estuary at a decadal timescale by applying a process-based model system (Delft3D), but their study only considered sand–mud mixtures and the variations of river water discharge and sediment discharge. A recent study noted that the 1-D modeling has difficulties in estimating actual sediment transport due to the meandering pattern of the river and emerging channel bars [24]. Such modeling work cannot be successful without detailed bedform information, which is essential for determining roughness and resistance of bed in modeling studies. Li et al. [25] found an average sediment inflow of 139 Mt/yr and an average sediment outflow of 32 Mt/yr from the Three Gorges Dam, showing an annual sediment trapping of 107 Mt (i.e., 77%) by the dam. The modeling study by Xie et al. [26] reported that the last 500 km reach of the Yangtze River (from Datong to Xuliujing) had not yet achieved a hydro-morphological equilibrium and the riverbed down-cutting was going to continue. However, the study did not analyze channel dynamics downstream of Wusongkou, i.e., the South Channel and South Passage. In the past, the South Channel and the South Passage (SCSP) were studied separately [27,28], though little work has been conducted on the entire channel. Although, according to [29], they determined the riverbed erosion/deposition rate of the South Channel and South Passage at a decade scale from 1997 to 2007. However, it is unclear what changes have taken place in the SCSP in the last decade. Therefore, the SCSP offers a typical case to determine a morphological adjustment in the deltaic channel with near-end engineering and basin dams for the current Yangtze delta.

This study focused on three questions: (1) Is there any recent change in channel dynamics of the lowermost Yangtze River, especially below Wusongkou in the Yangtze Delta? (2) Where is the eroded sediment from the Yangtze River deposited (in the estuarine channels or nearshore)?; (3) How long will the previously reported erosion in the Yangtze deltaic channel continue till an equilibrium state? To answer these questions, we combined

historical bathymetric surveys, high-resolution multibeam echo sounder data, discharge flow, tidal level, and sediment load to analyze recent morphodynamic evolution of the SCSP and the possible impacts of anthropogenic forcing on the evolution. Specifically, the objectives of the study were to: (1) investigate changes in the elevation and slope gradient along the channel thalweg in the SCSP during 1983–2018; (2) quantify changes in sediment volume along the channel before and after the closure of the Three Gorges Dam; (3) quantify the bed microtopography and basic flow properties along the channel thalweg of the SCSP; and (4) discuss the possible dominant factors of the transition in the modern Yangtze deltaic channel. Beyond its scientific purpose, the investigation of spatiotemporal geomorphic adjustment of the SCSP from this study has practical implications for the response of deltaic channels to the combined effects of changes of upstream water-sediment regimes and intensive human activities. It can also serve as an example for the remediation and development of other estuaries under similar natural and anthropogenic stresses.

2. Study Area

The Yangtze River is the world's fourth-largest river in terms of annual sediment load with a total draining area of 1.8 million km² [30] (Figure 1A). The Yangtze River Delta (Figure 1B) is one of the world's largest river-tidal systems with rapidly changing hydrology and morphology after the construction of many dams upstream. The Yangtze River Estuary is a multi-channel estuary with a three-level bifurcation and four distributaries separated by islands or banks [31]. Specifically, it is divided first into two branches separated by the Chongming Island: The North Branch and the South Branch (Figure 1B). The South Branch is further divided into the North and South Channels by the Changxing Island and the Hengsha Island. The South Channel (SC) is, again, further divided by the Jiuduansha Shoal into the North Passage and the South Passage (Figure 1B). The South Channel and South Passage are important shipping channels with intensive marine engineering equipment. The channels are developed from the South–North Channel bifurcation to the lower reach of the South Passage with a total length of about 80 km. The South Channel is a major conduit for Yangtze riverine sediment and flux with several canals including Changxing waterway, Waigaoqiao waterway, and Yuanyuansha waterway. The South Passage is a vital channel for vessels reaching the Shanghai Port. Datong Hydrological Gauging Station is located about 600 km upstream of the river mouth (Figure 1A), with the long-term discharge averaged at 29,300 m³/s [32].

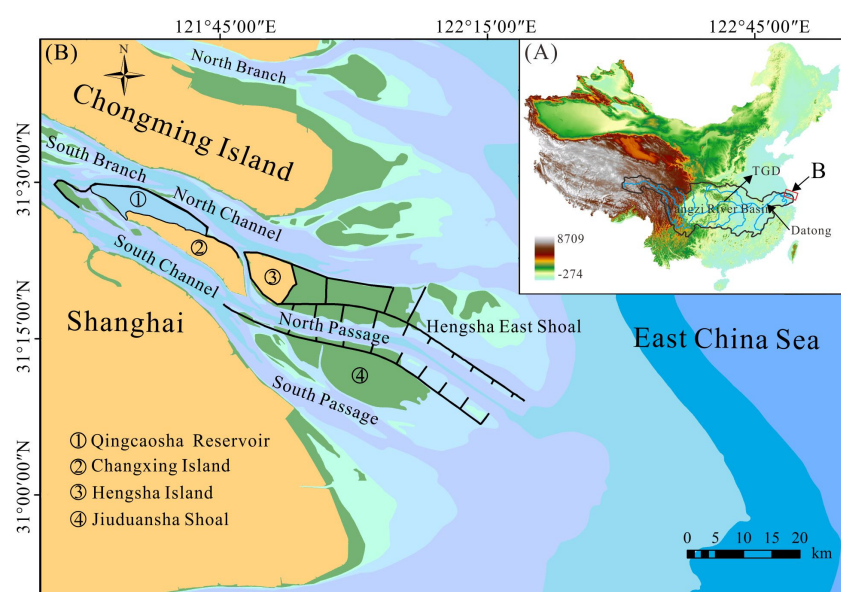


Figure 1. Cont.

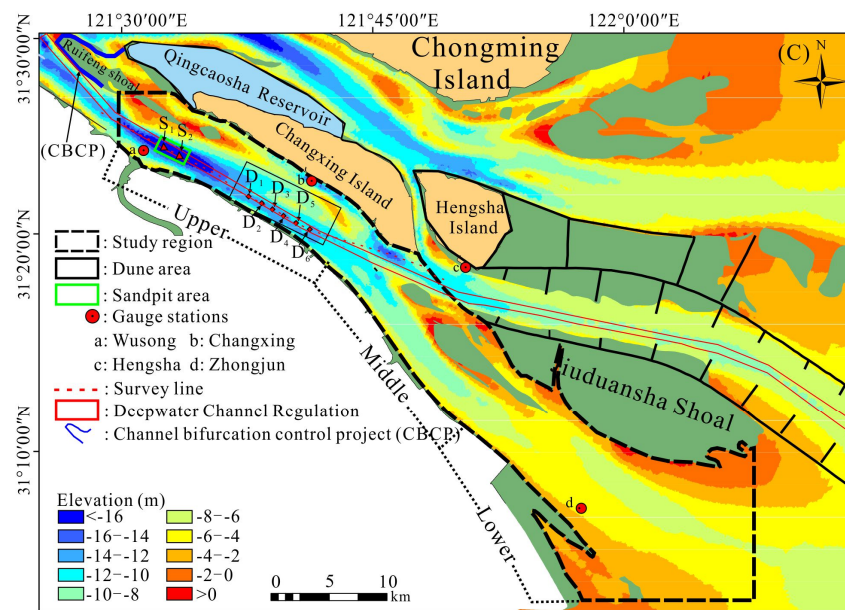


Figure 1. (A) Geographical location of the Yangtze River Basin in China. (B) the Yangtze River Estuary. (C) The study area: The South Channel and South Passage (SCSP).

3. Materials and Methods

3.1. Bathymetric Data Acquisition and Processing

In order to assess the morphological changes in the Yangtze River Estuary before and after the closure of the TGD, we gathered bathymetric records compiled by the Chinese Maritime Safety Administration (China MSA) in five different years from the past nearly four decades. These survey maps dating from 1983, 1998, and 2002 represent the bathymetric maps before the construction of TGD, while the charts from 2010 and 2018 reflect the geomorphic response after the closure and operation of TGD. The scale of the survey map in 1983 is 1:75,000 and the rest of the survey maps are on the scale of 1:25,000. These data built the foundation for the development of a digital elevation model (DEM) of the channels as described below. The coordinate system of raw bathymetric data was corrected to the ‘Wusong Datum’. Subsequently, the bathymetric data was georeferenced in Arc-GIS 10.5 software. To obtain a detailed estimation for channel elevations, the entire channel was divided into multiple sub-reaches, which represented a 1.6 km long reach in bankfull width. The kriging interpolation method, a widely used method in morphological change analysis of estuaries [4,12,33], was used to create DEMs with 50×50 m spatial resolution.

The bathymetric surveys were used to construct along-channel profiles. The location of the channel changed as it evolved, so the profiles were constructed along the position of the thalweg in that survey. These different along-channel profiles were normalized before comparison. Channel thalweg was defined as the lowest elevation point in each cross-section, which can be automatically acquired by the RBT tool in ArcGIS 10.5 [34]. Patterns of erosion and deposition are visualized using bathymetric difference maps, calculated by subtracting two survey maps by a plug-in software—Geomorphic Change Detection 7 in ArcGIS 10.5 software [35]. These difference maps were then used to estimate volumes of different erosional processes. The computed changes in riverbed topography were classified as depositional or erosional, depending on whether elevation increased or decreased, respectively.

3.2. Field Measurements

Field observations were made in the South Channel (Figure 1C). Measurements along the channel thalweg approximately 25 km long were taken over a semi-diurnal tidal cycle on 7 July 2018 (flood season) with the instrument assembly system including a small boat, the Seabat 7125 multibeam echo sounder (MBES), a dual-frequency acoustic Doppler

current profiler (ADCP, Rowe Technologies Inc.) and the EdgeTech 3100 sub-bottom profiler (Figure 2A). The operational frequency of MBES is 200 kHz/400 kHz. The central beam angle is 0.5° , and the maximum ping rate is (50 ± 1) Hz. It has 512 beams, and the theoretical depth resolution of 6 mm. The ADCP is used to obtain current velocity with the operational frequency of 200 kHz/400 kHz and the measuring range is ± 5 m/s. The high-resolution EdgeTech 0512i Chirp Sonar Subbottom Profiler was employed to obtain seismic data in the frequency range 0.5–7.2 kHz, at a ship speed of 4–5 kn (~ 7 –9 km/h). The position at a decimeter level of accuracy during the surveys was measured by a real-time Differential Global Positioning System (DGPS, Trimble) tied to a local navigation beacon with sub-meter accuracy. The horizontal accuracy is about 1 m and positioning accuracy is about 0.75 degrees. Surface sediment samples (about 3–10 cm) were collected from the SC during the survey using a grab (clamshell) sampler. In total, 6 riverbed sediment samples were analyzed in this study. The boat conducted the measurement along the survey line, which is the thalweg of the SC (Figure 1C), and the speed was controlled to be as steady as possible at 2.5 m/s. The weather conditions were good during the survey period.

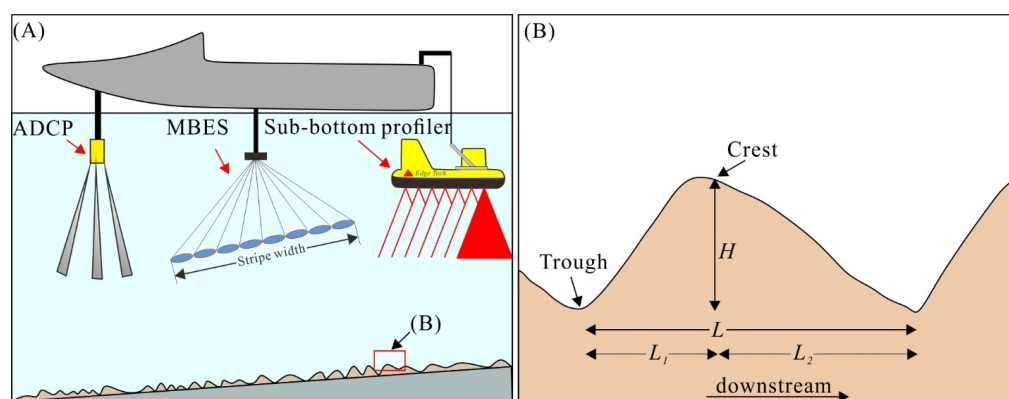


Figure 2. (A) Schematic diagram of instrument assembly related field measurements. (B) Definition of dune parameters.

The final multi-beam data was processed by draft correction, sound velocity correction, and roll, pitch, and yaw correction. The abnormal beam was removed in the editing module by PDS 2000 software (Teledyne RESON, Slangerup, Denmark). Tidal data at Wusong station were used for tidal correction. The collection mode was equidistant to ensure data uniformity in the acquisition module of the Teledyne PDS control center after considering and analyzing the above factors, the mapping resolution was 0.5×0.5 m. The grain size of sediment was determined in the laboratory using a Mastersizer 2000 laser analyzer (Malvern, Worcestershire, UK). The 10% H_2O_2 and 10% were used to remove Organic matter and $CaCO_3$ in the samples.

3.3. Evaluation of the Dune Characteristics

We collected parameters of dunes in this study including (1) dune length (L): the distance between two consecutive troughs (Equation (1)); (2) dune height (H): the distance of the crest from a straight line connecting two troughs, determined as a vertical line through the crest; (3) stoss-side slope length (L_1); (4) lee-side slope length (L_2), (5) dune index (L/H), and (6) the asymmetry (A), which is defined as the difference of the distance between the trough north of the crest and the distance between the crest and the trough south of the crest divided by the dune length (L) (Equation (2)) (Figure 2B).

$$L_D = L_1 + L_2 \quad (1)$$

$$A = (L_1 - L_2)/L \quad (2)$$

Bed roughness (K_s) of a river channel is mainly affected by form drag in sand, gravel, or sand-gravel bed rivers [36]. We estimated K_s associated with dune dimension by Van Rijn's (1984) approach (Equation (3)) examining the spatial distribution of bed roughness [36].

$$K_s = 1.1 * H_D \left(1 - e^{(-25 H_D/L_D)} \right) \quad (3)$$

where H_D is the average dune height in m, and L_D is the average dune length, in m.

3.4. Calculation of the Threshold Velocity of Dune and Bedload Transport Rate along the Channel Thalweg

The threshold velocity of sediment particles is one of the basic conceptions of river sediment dynamics. It is significant to the research on sediment movement and riverbed deformation [37]. There have been numerous formulas developed for estimating the initial velocity of sediment [38,39]. Zhang [40] developed the threshold velocity for granular and cohesive sediment, which is suitable for both coarse and fine. In a recent study, Guo et al. [41] estimated the initial velocity of the dune at the Yangtze River Estuary using Zhang's equation. In this study, we estimated the initial velocity of different dune groups along the channel thalweg with the equation developed by Zhang's formula, which is given as follows:

$$V_0 = \left(\frac{H}{D_{50}} \right)^{0.14} \left[17.6 \frac{\rho_s - \rho}{\rho} D_{50} + 0.000000605 \frac{10 + H}{D_{50}^{0.72}} \right]^{1/2} \quad (4)$$

where V_0 is the initial velocity of the dune; H is water depth; D_{50} is median grain size; ρ_s and ρ represents the density of water and sediment, respectively; in the natural sediment, $(\rho_s - \rho)/\rho = 1.65$. U is the average velocity.

Bedload transport is an important mechanism for sediment flux that could be used to examine the relationship between bedform evolution and net sediment transport [42]. There are numerous formulas for the bedload transport rate available, including Meyer-Peter's formula [43], Einstein's formula [44], and Ackers-White's formula [45]. They are concerned with the bedload transport rate, generally based on flume experiments under steady flow conditions or observations of natural rivers close to a uniform flow. Besides, Dune migration is the main form of bedload transport, bedload transport rate could be estimated via dune migration [41].

Zhang proposed a numeric relationship of relative wave height with Froude number and relative smoothness (Equation (5)) [41].

$$\frac{H_D}{H} = 0.086 \frac{U}{\sqrt{gH}} \left(\frac{H}{D_{50}} \right)^{1/4} \quad (5)$$

where H is the water depth, U is the average velocity; g is the gravitational acceleration (9.8 m/s^2), and D_{50} is the average median grain size.

Zhang also proposed the relation between relative dune migration velocity and average velocity by field-measured data as follows [41]:

$$\frac{C}{U} = 0.0144 \frac{U^2}{gH} \quad (6)$$

where C is dune migration velocity.

The volume of a dune (V) in a single width can be expressed as follows:

$$V = \alpha L_D H_D \quad (7)$$

where α is the volume coefficient, which is 0.5 due to the dune profile being approximated as a triangle.

Assume that the time required for the dune to migrate a distance of the length of the dune (L) is T , and the dry density of sediment is ρ , then the bedload transport rate per width in unit time (G_D) can be expressed as follows:

$$G_D = \frac{\alpha \rho L_D H_D}{T} \tag{8}$$

Because the dune migration rate (C) can be expressed as follows:

$$C = \frac{L_D}{T} \tag{9}$$

the bedload transport rate per width in unit time (G_D) can be expressed as follows

$$G_D = \alpha \rho H_D C \tag{10}$$

Combining Equations (5) and (6), the bedload transport rate per width can be written as:

$$G_D = \frac{0.00124 \alpha \rho U^4}{g^{1.5} h^{0.25} D_{50}^{0.25}} \tag{11}$$

where G_D is the bedload transport rate per width, U is the average velocity, g is the gravitational acceleration (9.8 m/s^2), ρ is the dry bulk density, 2650 kg/m^3 , and D_{50} is the average median grain size.

4. Results

4.1. Changes in Channel Thalweg and Channel Slope Gradient

The longitudinal profile of the SCSP showed an antislope, steady channel during the past three decades. The average thalweg elevation in the SCSP was -11.32 m , -10.04 m , -10.26 m , -10.04 m , and -11.05 m in 1983, 1998, 2002, 2010, and 2018, respectively. Concurrently, the average riverbed slope gradient of the SCSP was 0.09° , 0.04° , 0.06° , 0.06° , and 0.09° in 1983, 1998, 2002, 2010, and 2018, respectively. Compared with the seaward slopes (0.03° , 0.03° , 0.02° , 0.03° , and 0.04°) of the SCSP in the five years, the landward slopes were much greater (i.e., 0.12° , 0.07° , 0.1° , 0.09° , and 0.16°) (Figure 3A–E). The longitudinal changes of thalweg in the SCSP have undergone great changes during 1983–2018. These changes were mainly manifested in the substantial deposition in the upper sections of the SCSP with a maximum silt depth of $\sim 7.5 \text{ m}$. Conversely, the largest riverbed degradation occurred in its middle reach which is 38–40 km from the starting point, specifically, a 3.9 m deepening from -6.2 m in 1983 to -10.1 m in 2018. However, the morphology of the thalweg in the lower reach exhibited no significant change compared with the upper or middle reaches in the SCSP (Figure 3F).

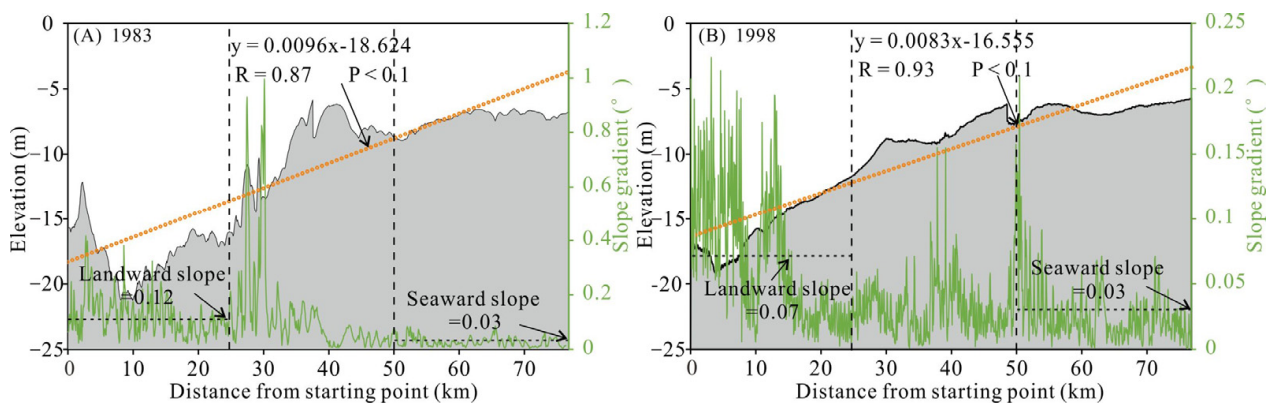


Figure 3. Cont.

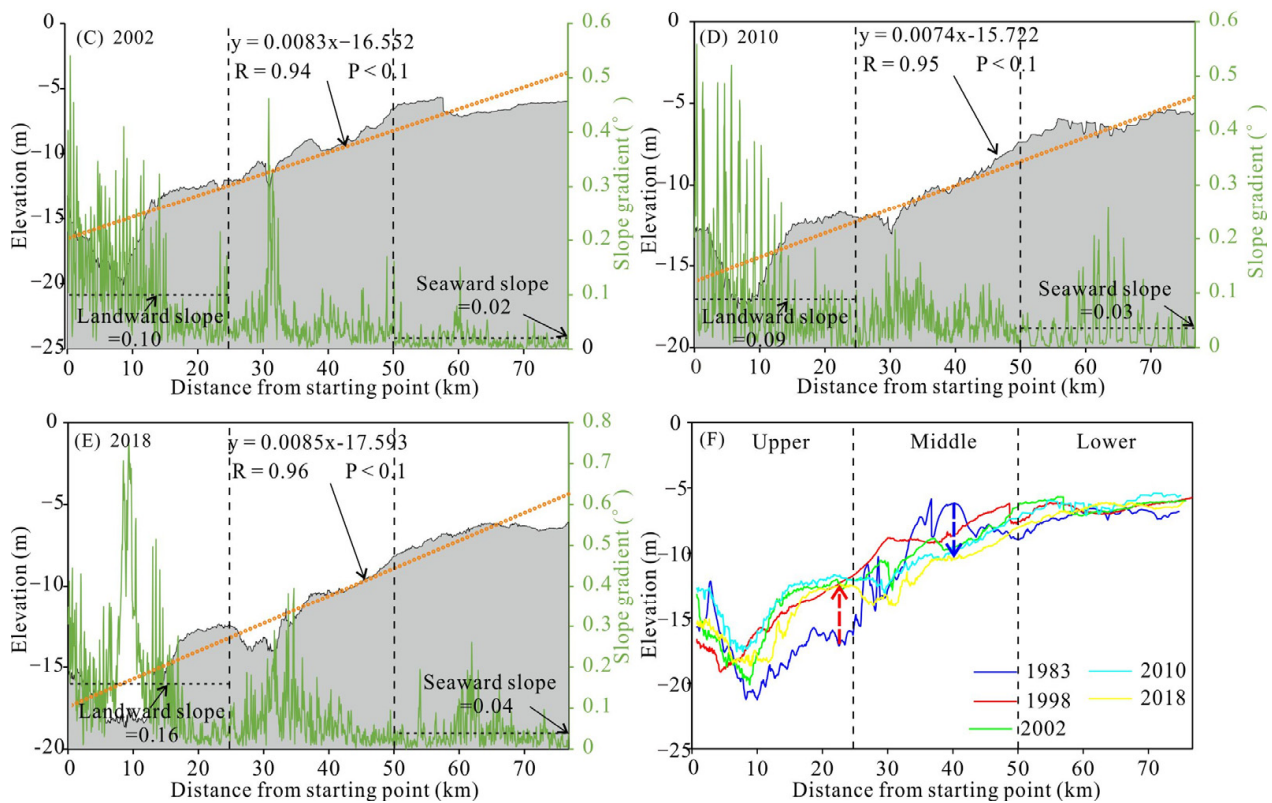


Figure 3. (A–E) The longitudinal profiles (black line) (left axis) and channel slope along the channel thalweg (green line) (right axis) of the Yangtze River Estuary during 1983, 1998, 2002, 2010, and 2018. (F) Changes in thalweg elevation of the Yangtze River Estuary during 1983–2018. The starting point of the horizontal axis is 4 km upstream of Wusong station (Figure 1C).

4.2. Spatiotemporal Variation of the SCSP Bed Elevation and the Riverbed Erosion and Deposition Patterns

Based on the survey charts between 1983 and 2018, a 3D contour map for the average bed elevation of the SCSP was constructed by kriging interpolation of average bed elevation values during the study period (Figure 4A) and the longitudinal profiles of the SCSP at different time are shown in Figure 4B. We found that there is no significant change in average bed elevation in the past 35 years along the entire 80 km deltaic channel. Specifically, the average bed elevation of the SCSP is -6.90 m, -6.67 m, -6.36 m, -6.83 m, and -6.84 m, respectively. However, we found that the upper boundary of maximum turbidity moves seaward (Figure 4B,C). Our assessment also shows that the SCSP has undergone excess riverbed deposition from 1983 to 2018 and the total amount of aggradation in the past 35 years over the entire length of the active channel is 1.62×10^7 m³. Specifically, there was a slight deposition with a net deposition rate of 0.91×10^7 m³/yr between 1983 and 1998 (Figure 5A). During 1999–2002, there was a sequential deposition with a net deposition rate of 3.31×10^7 m³/yr (Figure 5B). However, after 2002, the SCSP experienced significant erosion with a net erosion rate of 3.26×10^7 m³/yr during 2003–2010, and almost the entire river channel showed scouring except for the lowermost reach of the SCSP (Figure 5C). The riverbed shows slight bed aggradation with a net deposition rate of 0.09×10^7 m³/yr between 2011 and 2018 (Figure 5D).

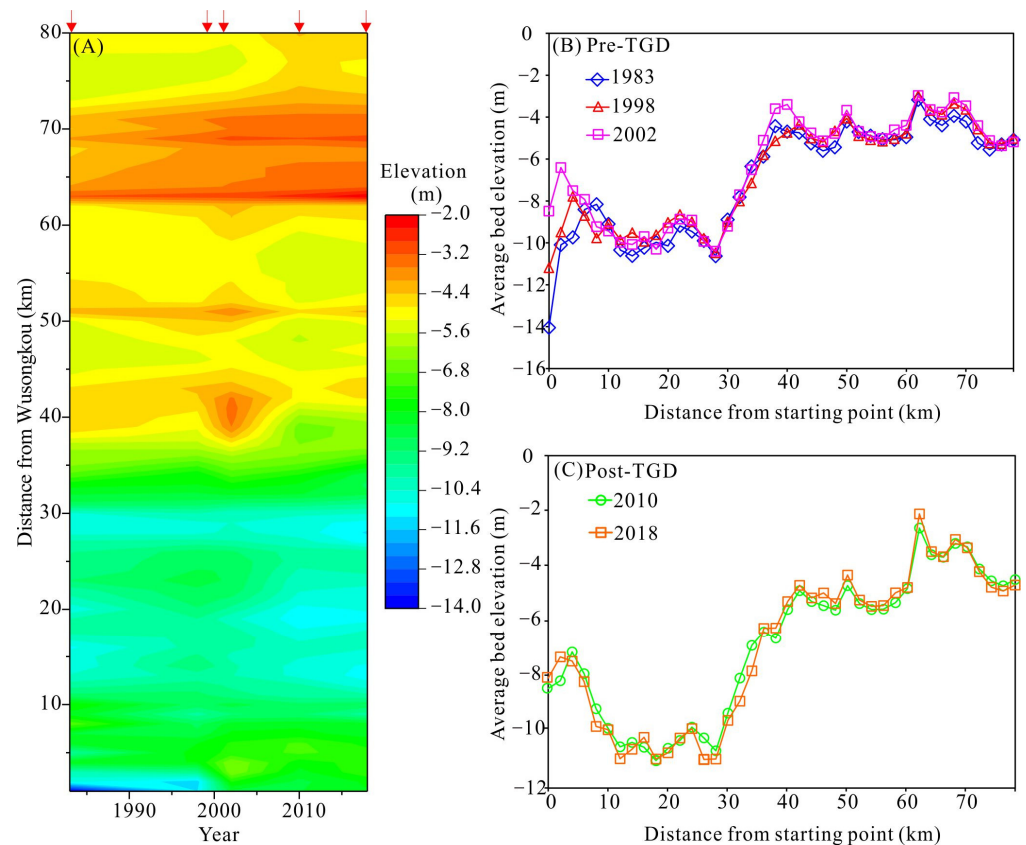


Figure 4. Spatiotemporal variation in bed elevation along the Yangtze estuary channel between 1983 and 2018. (A) 3D contour map. Red arrows correspond to the longitudinal profiles shown in panels (B,C). (B) Longitudinal profiles for different points in time before the closure of the Three Gorges Dam. (C) Longitudinal profiles for different points in time after the closure of the Three Gorges Dam.

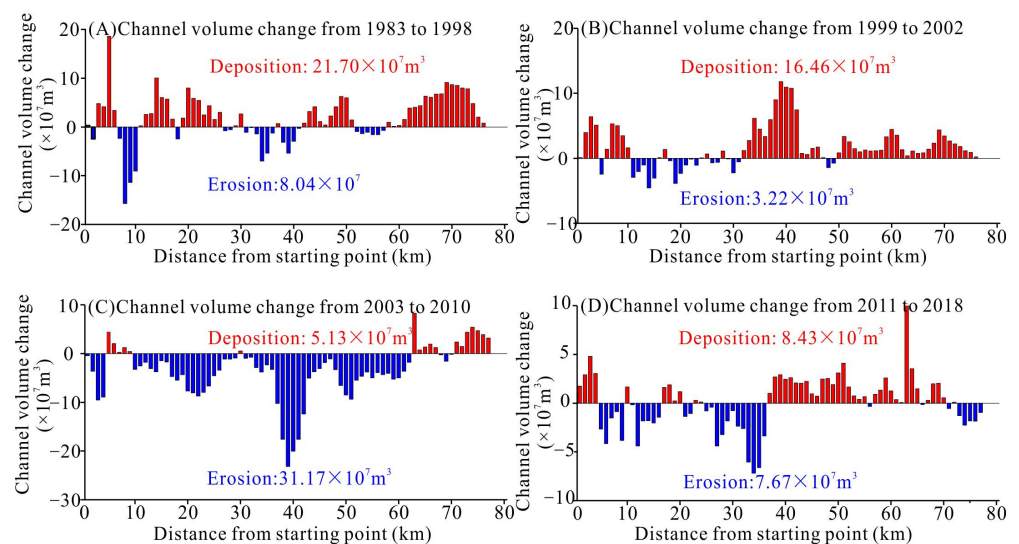


Figure 5. The SCSP channel dynamics over time. (A) Channel volume change in the SCSP from 1983 to 1998. (B) Channel volume change in the SCSP from 1998 to 2002. (C) Channel volume change in the SCSP from 2002 to 2010. (D) Channel volume change in the SCSP from 2010 to 2018.

4.3. Bed Microtopography along the Channel Thalweg in the South Channel

Our multibeam data show that dunes were the most common microtopography, accounting for 60.8% of the study area, while the flatbed accounts for approximately

35.6%. The rest is erosional topography (approximately 3.6%). Dune was the most widely developed riverbed micro-topography in the upper reach of SCSP. There is a dune group with a 7.5 km length in the upper reach of the SCSP (Figure 1C). The dune was well-developed in water depth between -11.8 m and -13.5 m. Small and medium dunes accounted for 99.2% of the dunes in the study reach (Figure 6B–G). In addition, scouring microtopography also was found and there is an amount of regular and oval regular sandpits located in the upper reach of the SC (Figure 1C). The multi-beam data showed that illegal sand mining holes are usually distributed on the margin of the navigation channel (Figure 7A). The length of the sandpit group is about 200 m, and they displayed an elliptical shape with a maximum diameter of 50 m and a maximum volume of $16 \times 10^3 \text{ m}^3$ (Figure 7B). These regular sandpits were about 1.8 m deeper than the surrounding bed surface (Figure 7B,C).

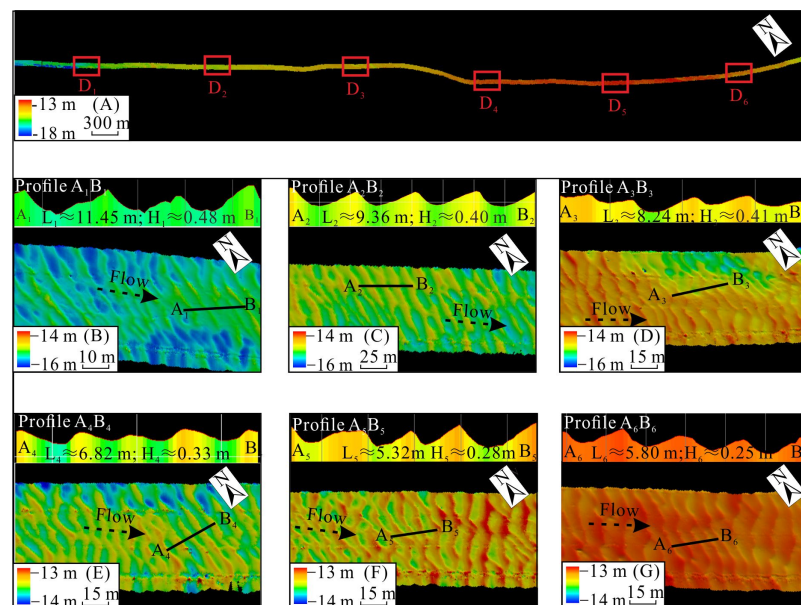


Figure 6. Diagram of the dune in the SC of the Yangtze River Estuary. (A) is the distribution diagram of the dune in SC with an inverse bed slope. D1–D6 represents the location of the dune group (Figure 1C). (B–G) are images of the morphology of the dune.

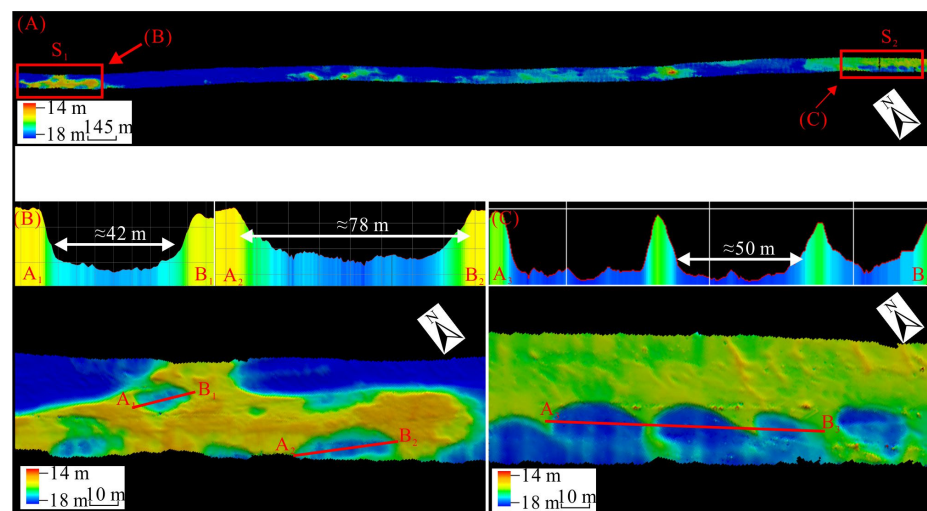


Figure 7. Diagram of the sand mining in the SC of the Yangtze River Estuary. (A) The distribution diagram of the dune in SC. S₁ and S₂ represent the location of the sandpit group (Figure 1C). (B) and (C) The images of the morphology of sand mining.

4.4. The Threshold Velocity of Dune and Bedload Transport Rate along the Channel Thalweg

The sub-bottom profile is about 12 km in the field measurement (Figure 8C). The result shows that the erosion structure and sediment accumulation were distributed alternately below a shallow depth of -13.5 m. During the survey period, the average flow velocity is 1.05 m/s, varying between 0.25 m/s and 2.85 m/s and the flow velocity increased from the left channel to the right channel (Figure 8A). We counted the morphology parameters of dune groups with the same interval (1.5 km). Morphological analysis of the dunes at the study site showed a dune length of 4.25 to 21.86 m with an average value of 7.87 m. The minimum, maximum, and average heights were 0.08, 0.65, and 0.36 m, respectively. The length/height ratio (L/H) of dunes varied from 16.23 to 25.89, and the mean was 21.70 (Table 1). We found that the average length and height of dunes increase correspondingly with the increase of water depth in the antislope channel. The threshold velocity along the channel thalweg has been increased with a fluctuation from 0.57m/s to 1.08 m/s with the decrease of water depth. Concurrently, the bedload transport rate has been increased from 0.05 kg/s to 0.19 kg/s with the decrease in water depth. The bed roughness (K_s) associated with the dunes varied from 0.18 to 0.34 (Table 1). Dunes presented a greater value of K_s (0.34) occurred in the deeper area across the river channel, while a much smaller value of K_s (0.18) occurred in the shallow area. The sediment was collected simultaneously during the field measurement and the analysis result shows that the grain size of the sediments in the dune group channel becomes finer towards the section downstream of the channel (Table 1).

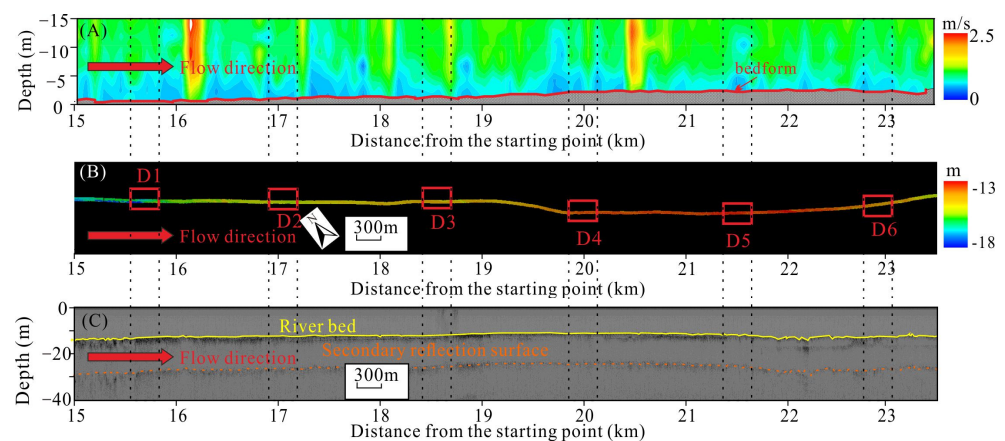


Figure 8. (A) Velocity profile along the SC (RK 15.5-RK 23.0). (B) MultiBeam echo sounder bathymetry. (C) Sub-bottom profile in the part of SC.

Table 1. Characteristics of the riverbed dunes in the SC of the Yangtze River Estuary with inverse bed slope.

Location	RK	H (m)	D_{50} (μm)	L_D (m)	H_D (m)	L/H	A	U (m/s)	G_D (kg/s)	V_0 (m/s)	K_s
D1	15.5	15.5	156	11.45	0.48	23.85	0.45	0.66	0.05	0.57	0.34
D2	17.0	14.9	115	9.36	0.40	23.40	0.41	0.68	0.03	0.71	0.29
D3	18.5	14.5	68	8.24	0.41	20.09	0.36	0.70	0.07	0.72	0.21
D4	20.0	13.6	49	6.82	0.33	20.67	0.32	0.71	0.08	0.81	0.26
D5	21.5	13.3	37	5.32	0.28	19.00	0.29	0.75	0.12	0.91	0.23
D6	23.0	13.1	25	5.80	0.25	23.20	0.26	0.83	0.19	1.08	0.18

Note: The location of the dune group is shown in Figure 1C. RK is the distance from the starting point. H is the average water depth; L_D is the average length of the dune; H_D is the average height of the dune; D_{50} is the average median grain size; G_D is bedload transport rate per width; V_0 is the threshold velocity of the dune; K_s is the average bed roughness.

5. Discussion

5.1. Impacts of Variations in Flow and Sediment Regimes

In recent decades, suspended sediment loads in the YR have changed significantly [13,30,46,47]. In particular, following the closure of the Three Gorges Dam in 2003, the annual sediment load at Datong station showed a great decreasing trend by nearly 70% from 1955 to 2018, while the river discharge remained relatively unchanged (Figure 9A). With substantial suspended sediment trapped in the Three Gorges Reservoir, downstream sub-saturated flow caused remarkable erosion of the riverbed in the lower YR [4,48]. The cumulative erosion volume in the bankfull channel was $468 \times 10^6 \text{ m}^3$ from 1998 to 2013 [4]. Nonetheless, the evolution processes of the SCSP during 1983–1998, 1999–2002, 2003–2010, and 2011–2018 were (1) deposition, (2) significant deposition, (3) severe scouring, and (4) light deposition. During 1983–1998, the SCSP displayed slight deposition with a net deposition volume of $1.36 \times 10^8 \text{ m}^3$ under an average annual sediment load of $3.74 \times 10^8 \text{ t}$ at Datong (Figure 9B). During 1999–2002, the river channel still displayed a slight deposition with a net deposition volume of $1.32 \times 10^8 \text{ m}^3$. According to [49], this sediment value was only 79.6% of the average value during 1951–1985 ($4.70 \times 10^8 \text{ t Mt}$). It indicates that the decrease of sediment inflow from the upstream has no significant effect on the downstream channel during the period. During 2003–2010, the sediment load decreased quickly due to the construction of the TGD in 2003, the average sediment load was decreased to $1.64 \times 10^8 \text{ t}$ (Figure 9A), which was 47.1% of the average sediment load ($3.48 \times 10^8 \text{ t}$) in 1983–2002. Subsequently, the SCSP exhibited a severe scouring with a rate of $2.60 \times 10^8 \text{ m}^3$ each year. Thus, it appears to be credible that the decrease in sediment load leads to the natural erosion of the river channel. During 2011–2018, the average sediment load still reduced to a low level ($1.24 \times 10^8 \text{ t}$) and the discharge at Datong station showed no obvious change (Figure 9A), however, the SCSP remain a stable state with a slight deposition of with net deposition of $0.07 \times 10^8 \text{ m}^3$. According to [12], there is obvious erosion during 2012–2016 in the offshore area of the North Channel.

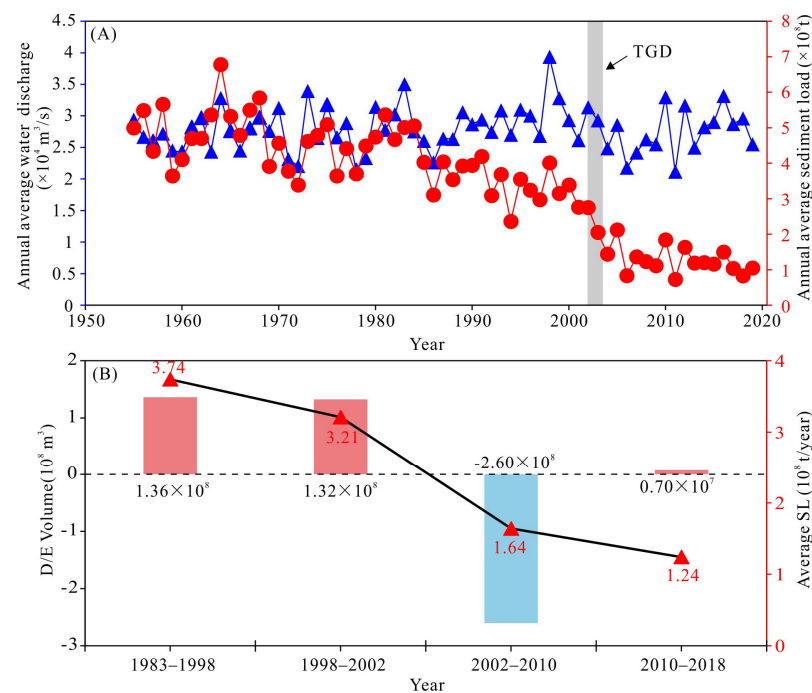


Figure 9. (A) Average annual discharge (left axis) and suspended sediment load (SSL) (right axis) at the Datong station from 1955 to 2018. (B) The correlation between the annual sediment load at Datong and the annual volume change in the SCSP. The long-term suspended sediment loads and river discharge were obtained from the Yangtze River Sediment Bulletin (published on <http://www.cjh.com.cn>, accessed on 1 January 2022). Note: TGD means the Three Gorges Dam.

The ebb flow/sediment diversion ratio of the SC/SP during 1998–2017 showed that there is little difference between the ebb flow diversion ratio and ebb sediment diversion ratio in SC (Figure 10A). However, in the last 10 years, the ebb sediment diversion ratio of the SP (i.e., 64%) is greater than the ebb flow diversion ratio (i.e., 57%) (Figure 10B). This indicates that a lower flow ratio can result in bed silting in the mainstem channel owing to insufficient stream power (Figure 5D). On the other hand, a larger diversion flow ratio brought more sediment to this area, and the mouth bar had not yet been eroded due to the lack of engineering projects, which maybe one reason why the bar in SP had a large volume [27]. Previous research [21] has shown that the sediment in the Yangtze Estuary comes from both the land and the sea by the analyses with the particle sizes of bed materials. They also suggested that the available fine sediment supplied to the estuary from the offshore area is abundant. Thus, the accretion of the SCSP could be reliant on sediment sources from the upstream and offshore areas of the SC during the period. In combination, it indicated that the deltaic channel evolution of the SCSP does not correspond to the yearly riverine sediment and discharge at Datong station positively. It can be concluded that although the reduction of sediment load can lead to the overall erosion of the river channel at the macro scale, other causes need to be considered during the evolution of the SCSP.

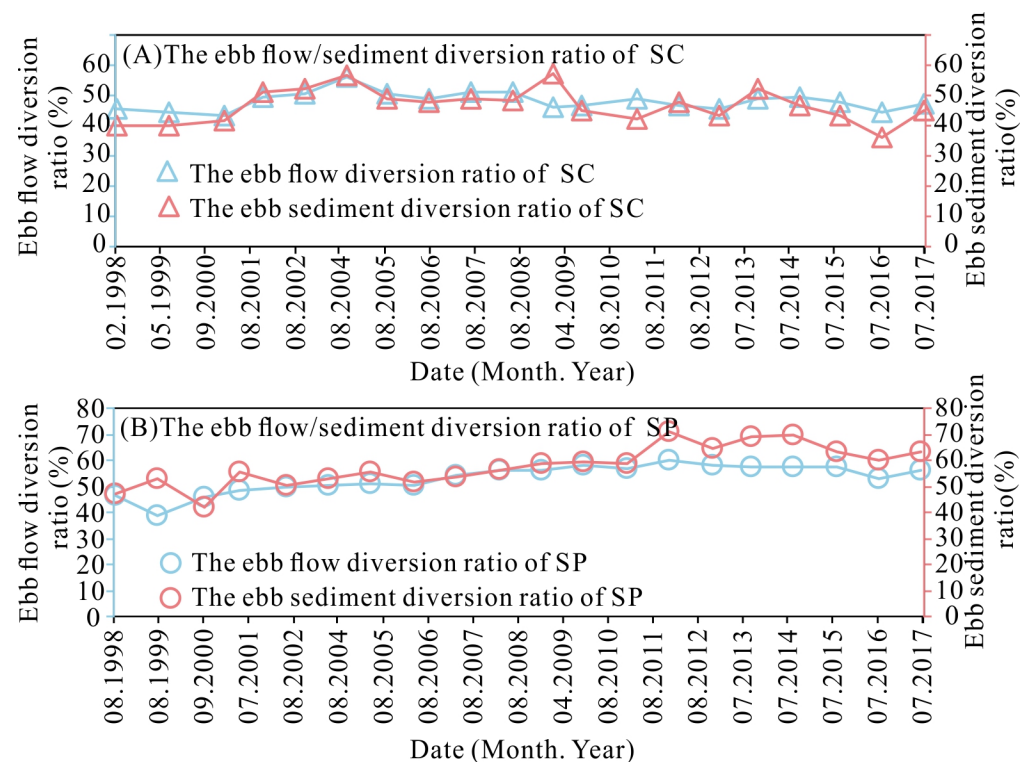


Figure 10. (A) Ebb flow/sediment diversion ratio of the SC during 1998–2017. (B) Ebb flow/sediment diversion ratio of the SP during 1998–2017. (Note: The data about the ebb flow/sediment diversion ratio of the SP during 1998–2017 were collected by the Changjiang Estuary Waterway Administration Bureau CJWAB).

5.2. Impacts of Tidal Processes and Human Intervention

Global sea level has been rising, which can affect sediment transport in the backwater zone of a lowland alluvial river [20]. Consequently, a high rate of deltaic sedimentation can be a response to the accelerated sea-level rise in recent decades [50]. Cheng et al. [51] reported that variations in annual mean sea level (MSL) from 1996 to 2011 at the main tidal gauge stations in the Yangtze Estuary show a significant mean sea level rise (MSLR) ranging from 8 cm to 10 cm. According to [52], the intrusion of the tide during low discharge can also produce seasonal sediment deposition in a tidal estuary.

The studied channel showed a downstream tract with seaward-decreasing depth, mainly controlled by the tidal dynamics (Figure 3). Tidal processes tend to lead to a landward net transport with sediment import, which is more effective during the low discharge. The role of tides is also confirmed by the obvious landward net transport in channels with low or no river discharge [53]. Gugliotta and Saito [53] pointed out that with the increase of tidal energy, the channels of tide-dominated river deltas may become shallower. In our study, the annual lowest tidal level in the Wusong, Changxing, Hengsha, and Zhongjun stations (Figure 1C) along the SCSP presented a sharp increasing trend (Figure 11). For instance, the lowest tidal levels at Wusong rose from 8 cm to 34 cm from 1993 to 2018 (Figure 11). Thus, the increased tidal energy may accelerate the siltation of sediments in the lower reach of the SCSP. We suggest that in the future, hydrodynamic modeling should assess the responses of the deltaic channel to tides.

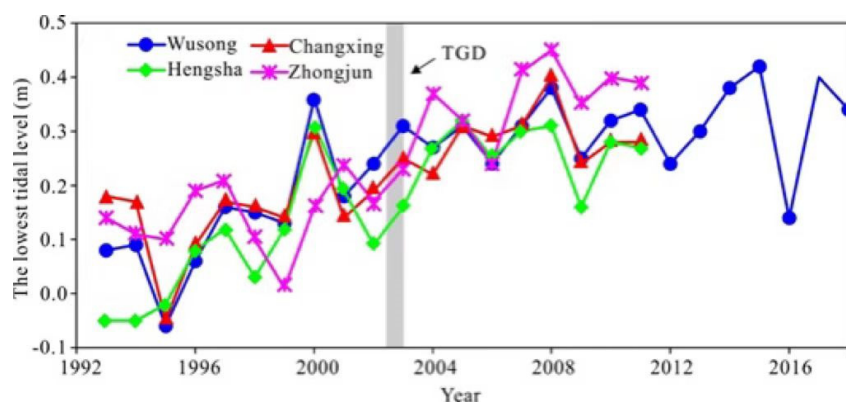


Figure 11. Annual lowest tidal level at Wusong, Changxing, Hengsha, and Zhongjun in the Yangtze River Estuary from 1992 to 2018). Note: the tidal level was obtained from Shanghai Municipal Oceanic Bureau (<http://swj.sh.gov.cn/>, accessed on 1 January 2022).

The influence of local engineering on river channel evolution is mainly reflected by the change in river channel boundary conditions and the dynamic sedimentary environment of regional river channels [54]. For example, the construction of the Qingcaosha Reservoir in the Yangtze River Estuary has narrowed the channel width and led to channel erosion from 2002 to 2012 in the North Channel [12]. Xu et al. [6] reported that local engineering projects on the Nanjing reach resulted in the siltation of the near bank in the tidal channel of the YR. In the study, we also found significant erosion in the uppermost reach of SC during 2002–2010 (Figure 5C). During 2007–2009, the North–South channel bifurcation control project (Figure 1) not only stabilized the pattern of the barbody in the North–South channel bifurcation but also affected the flow-sediment ratio that run into the SC [55]. According to [56], the ebb flow ratio into the SC decreased from 56.2% in 2002 to 45.2% in 2009, and the sediment ratio into the SC increased from 41.1% in 2002 to 56.5% in 2009. These indicated that the sediment transport capacity of the flow is weaker in the SC than in the NC, as a result, the uppermost reach of SC experienced a slight deposition with the disproportional flow-sediment ratio (Figure 5D). Although the sediment load appeared to have declined quickly (Figure 11). The SCSP has been affected by the Deepening Waterway Project (Figure 1C) carried out between 1998 and 2010, which has narrowed the channel and caused banked-up water over a large area of land reclamation by siltation [52]. Concurrently, the SC has been continually dredged to the present 12.5 m using trailing-suction hopper dredgers [57]. According to the [58], the back siltation increased obviously in the waterway. To maintain a deep waterway, dredging must be carried out continually and a large of dredging marks and hollows have become apparent in recent years in the SC (Figure 8B,C). According to [53], the reported human-induced narrowing and deepening have certainly changed the channel depth and width at numerous sites, but they have not altered the general trends of constant width to seaward widening and seaward deepening to seaward-shallowing trends, as these remain evident in data from different decades. Zheng et al. [4]

pointed out that the change in channel width mainly occurred in the lower reach of the Lowermost Yangtze River. Specifically, the channel width of the river reaches from RK 130 to RK 30 decreased by 1.6 km upstream of Wusong. In this study area, spur dike construction and reclamation projects have narrowed the NP, leading to the discharge from the SC tending to flow through the SP. Subsequently, the diversion ratio of the SP increased. A study by [59] reported a sand mining volume of 10 million cubic meters from 1998 to 2006. In our study, the total volume of erosion in the entire SC was about 128 million cubic meters during 1998–2010 (Figure 5B,C), suggesting that the mining effect on the erosion of the upper reach of the SCSP is rather limited. During the study period, several severe floods occurred during typhoon storms such as Typhoon Winnie in 1997 and Typhoon Matsa in 2005, as well as during Typhoon Nepartak in 2016 [60]. Extreme events of storm surges and frequent strong winds may have caused significant short-term fluctuations in the erosion/deposition of the deltaic channel in the recent study [5].

5.3. Relationship between Dune Development and Channel Morphodynamics

Subaqueous microtopography is a general type of bedform in deltaic channels and is closely related to local hydrodynamic conditions, water depth, and sediment grain size [61–63]. We found numerous dune groups that had developed between the scouring area and the sitting area in the middle reach of the SC (Figure 7). Wu et al. [27] also reported a large area of dunes on the south side of the upper reach of the SP. As proposed by Wang et al. [64], the channel-scale topography is related to the development of small-scale topography. Thus, the stability of the channel can be reflected by the movement of dunes. In this study, the threshold velocity of the dune at D1 gradually increases along the channel from 0.57 to 1.08 at D6 (Table 1), while the sedimentary processes of the channel gradually changed from siltation to scour (Figure 5D), which indicates that the threshold velocity of the dune in the scouring area is smaller than that in the siltation area. Combining the sediment transport rate, we found that the sediment in the scouring area was transferred to the siltation area (Figure 6C). Paarlberg et al. [65] noticed that dune roughness was linearly related to dune height. This may explain our finding why a much higher value of k_s occurred in the shallow water (0.34) when compared with dunes in the deep water (0.18) (Table 1). Our study showed that the mean grain size of bed sediment decreases downstream in the Yangtze River Estuary (Table 1), which may have resulted in the smaller dunes in the channels. The finding is in good agreement with those recently reported by Wu et al. [66] for the lower Lowermost Mississippi River.

The morphology of dunes can be related to several factors including flow conditions, sediment supply, and bed materials. Dunes are generally formed in coarse particle deposition areas [67,68]. In the past three decades, a total of approximately $1.11 \times 10^8 \text{ m}^3$ of sediment was deposited within the SCSP (Figure 5), providing sufficient sediments for the development of dunes. Unsworth et al. [69] stated that the dominant effect of dunes on sediment transport direction is through their influence on near-bed flow direction, with a secondary effect linked to their impact on the depth-averaged flow. The riverbed is flat with a relatively low flow velocity. In contrast, bedform scouring occurs when the flow velocity is considerably high [70]. The SCSP is affected by river flow and tidal currents simultaneously. Thus, its hydrodynamic condition is highly complicated. The results of the hydrodynamic along the channel thalweg show that the average flow velocity is 0.79 m s^{-1} , and the average velocity near the bed is about 1.57 m s^{-1} (Figure 6C). These flow conditions are also beneficial for the development of dunes according to [71]. River channels with narrow, straight, and certain water surface slopes are facilitating the development of large dunes by constraining stream power [68]. In this study, the deltaic channel has developed an antislope channel of about 80 km in length (Figure 6). Concurrently, compared with the seaward slope (0.03° , 0.03° , 0.02° , 0.03° , and 0.04° , respectively) in the SCSP, high slope landward slope (0.12° , 0.07° , 0.10° , 0.09° , and 0.16° , respectively) obviously occurred in the study year. (Figure 3A–E). According to Southard and Boguchwal [72], a larger riverbed gradient may lead to channel incising, which may result in the coarsening of sediment

and larger dunes. This may explain why the larger grain size of bed sediment occurred mainly in the upper reach of the SCSP. Previous studies have also shown that the mean grain size of bed sediment (Table 1) decreases along the channel thalweg in the SCSP [33]. Consequently, these may be closely related to the decrease in the length of dunes along the channel thalweg in the SCSP (Table 1 and Figure 6B–G). Our results demonstrate that the length of dunes depicts an increasing trend in the SCSP from upstream to downstream and the general bed slope gradient is high. This verifies that the large bed slope is one of the key factors in dune development; specifically, the inverse bed slope is more beneficial to the development of dunes under the control of river flow, and this expands our new understanding of the control factors of dunes morphology. Further studies on the correction formula for the dune length are needed to help understand the deformation of dunes.

5.4. Implication for Other Deltaic Channels

Based on the evolution phases, we propose a conceptual model for the morphological adjustment of the SCSP (Figure 12). The model identifies several distinct patterns, which can be classified into the growing phase, erosion phase, and transformation phase. During phase I from 1983 to 2002, massive sedimentation occurred in the entire channel. Bed slope decreased rapidly due to channel progradation and the downstream-increasing sedimentation rates (Figure 12). During phase II from 2003 to 2010, average annual discharge and sediment load decreased by 6.9% and 61.5% compared with phase I, concurrently, the landward slope decreased, yet the seaward slope increased during this time. The main channel deepened rapidly under the impact of decreased sediment load due to the closure of the Three Gorges Dam in 2003, highlighting channel responses to specific human activities (Figure 11). At the final stage of becoming stable, the average annual discharge increased by 4.6%, while the annual sediment load decreased by 24.6%. The SCSP did not vary significantly, keeping the balance of scouring and silting, compared with fluxes in phase II (Figure 11). Following the slower development pace of engineering projects after 2010, the stable diversion ratio may have helped the SC remain in a stable state [54]. At the same time, with stronger tidal forcing and sea level rise (Figure 11), the volume of the seaward reach of the SCSP kept slightly increasing. The evolution phases in Figure 12 may be different from those proposed by other experts, which considered evolution or subaerial and subaqueous YRD [12,28,73]. For example, according to [12], another deltaic channel (North Channel) in the Yangtze River Estuary experienced opposite erosion and deposition patterns. Specifically, the river regime evolution processes of the NC during 1986–2002, 2002–2007, 2007–2012, and 2012–2016 were severe scouring, light deposition, slight scouring, and scouring, respectively. However, a similar finding is that the NC has been stable in the last 10 years, whose erosion rate is marginal ($0.40 \times 10^7 \text{ m}^3$).

The geomorphologic process of the deltaic channels investigated in this study is comparable with other world large river deltaic channels, such as the Yellow River deltaic channel, Mekong deltaic channel, Mississippi River deltaic channel, and Atchafalaya River deltaic channel, where similar studies have been conducted [24,74–76]. As one portion of a deltaic system, the evolution processes of deltaic channel are all highly impacted by variations of discharge, sediment load, and human intervention. Phase I of the rapid aggradation in the Yangtze River Estuary may be a common, immediate response for rivers to abrupt avulsions, especially rivers with high sediment load [77]. However, different from those studies, our findings indicate that the YRD channel has experienced the morphology transformation from severe riverbed erosion to a stable state under anthropogenic interferences (Figure 11). The difference can be explained by the fact that a large number of near-end engineering projects have been built in the Yangtze Estuary over the past several decades [12]. As a result, these engineering projects changed the river boundary of the deltaic channels, and the morphological evolution of the deltaic channels has been impacted. Concurrently, we found that dunes have the most common morphology in the SCSP, and the inverse bed slope is more beneficial to the development of dunes under the control of runoff, which expands our new understanding of the control factors of dunes morphology.

In the 21st century, human activities are largely responsible for the vulnerability of deltaic channels. The number of natural distributary channels on deltas has often been reduced artificially to control deltaic channels' location and protect populated areas by levees [78]. A common consequence is the super-elevation of the riverbed above the delta floodplain. In combination, processes of delta subsidence and channel bed aggrading are a threat to the societies and ecosystems that they support. Our results obtained from this study on the redistribution of water and sediment load in the YRD can provide scientific guidelines for water and sediment reallocation in the future.

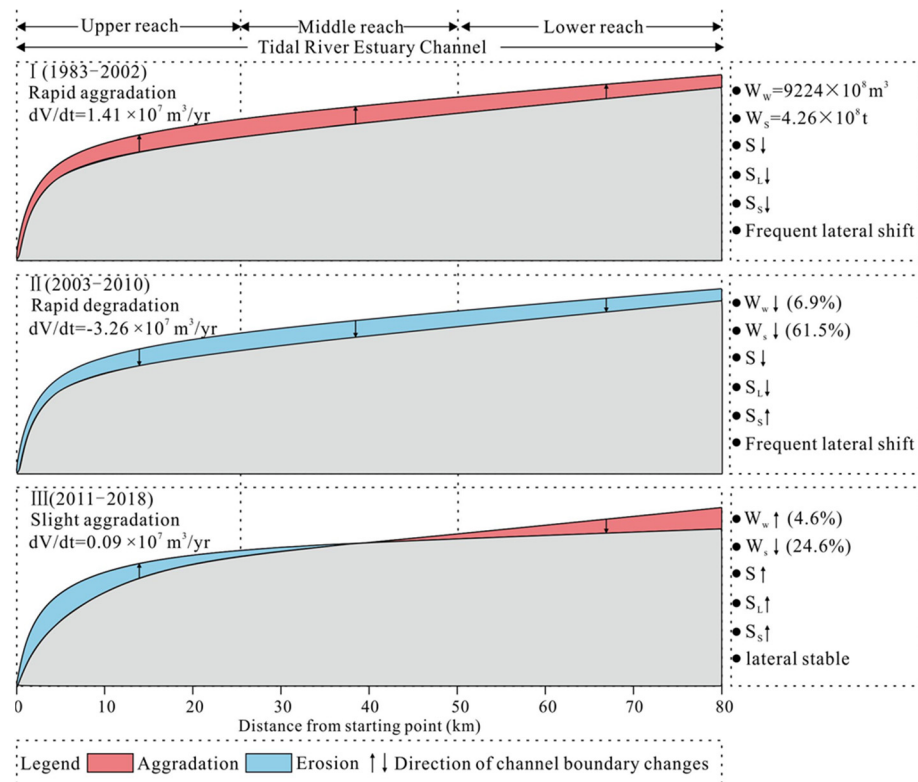


Figure 12. A conceptual model for the morphological adjustment of the SCSP. Note dV/dt = channel volume change rate. Positive values mean deposition and negative values mean erosion. W_w and W_s = average annual discharge at Datong station and average annual sediment load at Datong station. S = channel slope, S_L = landward slope, S_S = seaward slope. \uparrow and \downarrow denote the increase and decrease of a geometric parameter, respectively.

6. Conclusions

Our long-term assessment on the morphologic changes in the Yangtze River Estuary channels offers a field case study to inform the far-reaching impact of damming river. The evolution of these estuarine channels can be characterized by three phases: Phase I (1983–2002)—a channel aggradation of $1.4 \times 10^7 m^3/yr$; Phase II (2002–2010)—a rapid channel erosion of $3.26 \times 10^7 m^3/yr$; and Phase III (2010–2018)—a relatively steady transition showing a marginal deposition of $0.09 \times 10^7 m^3/yr$, implying the trend to a new state of dynamic equilibrium. The closure of the Three Gorges Dam in 2003 has played a key role in riverine sediment decline, forcing the deltaic channel to adjust at the macro scale. The anthropogenic activities including the nearby river engineering project and sand mining have exerted additional influences at the micro-scale, whereby dunes show the most common morphology throughout the channel riverbeds. Based on the findings, we conclude that the lowermost estuarine reach of the Yangtze River is transferring from erosive to depositional, and that this trend will likely accelerate as the sea level continues to rise. These findings advance our understanding of estuarine channel development in

response to upstream human intervention, providing insights for developing sustainable management of the Yangtze River Delta and other river deltas in the world.

Author Contributions: Conceptualization, H.C. and Y.X.; methodology, M.T.; software, M.T.; validation, M.T., H.H. and B.W.; formal analysis, M.T., H.H., B.W. and S.Z.; investigation, M.T., L.T. and W.X.; resources, H.C.; data curation, M.T. and E.Z.; writing—original draft preparation, M.T.; writing—review and editing, M.T., H.C., Y.X., Z.Y. and J.L.; visualization, M.T.; supervision, H.C. and Y.X.; project administration, H.C. and Y.X.; funding acquisition, M.T., H.C., Y.X. and H.H. All authors have read and agreed to the published version of the manuscript.

Funding: This study was financially supported by a NSFC-NWO-EPSRC (grant number 51761135023), Natural Science Foundation of China (grant number 42201009), Education Department of Jiangsu Province (grant number 22KJB170022), and the Impact of Major Projects on the geological environment of the Yangtze River (Grant No. DD20160246). During the preparation of this manuscript, Ming Tang was supported by an award from the East China Normal University scholarship program for graduate students, and Y. Jun Xu received funding support from a U.S. National Fish and Wildlife Foundation project (award 1212112) and a U.S. Department of Agriculture Hatch Fund project (LAB94459).

Data Availability Statement: The bathymetric data used in this study can be obtained from the Chinese Maritime Safety Administration. Processed data are available upon request to the lead author.

Acknowledgments: The authors thank the Chinese Maritime Safety Administration for making the long bathymetric survey data available for this study. The authors are also grateful to two anonymous reviewers and the editor, whose thoughtful comments and suggestions helped improve the manuscript.

Conflicts of Interest: The authors declare no conflict of interest.

References

1. Walling, D.E.; Fang, D. Recent trends in the suspended sediment loads of the world river. *Glob. Planet. Chang.* **2003**, *39*, 111–126. [[CrossRef](#)]
2. Nilsson, C.; Reidy, C.A.; Dynesius, M.; Revenga, C. Fragmentation and flow regulation of the world's large river system. *Science* **2005**, *308*, 405–408. [[CrossRef](#)] [[PubMed](#)]
3. Meade, R.H.; Moody, J.A. Causes for the decline of suspended-sediment discharge in the Mississippi River system, 1940–2007. *Hydrol. Process.* **2010**, *24*, 35–49. [[CrossRef](#)]
4. Zheng, S.W.; Xu, Y.J.; Cheng, H.Q.; Wang, B.; Xu, W.; Wu, S.H. Riverbed erosion of the final 565 kilometers of the Yangtze River (Changjiang) following construction of the Three Gorges Dam. *Sci. Rep.* **2018**, *8*, 11917. [[CrossRef](#)] [[PubMed](#)]
5. Wang, B.; Xu, Y.J. Estimating bed material fluxes upstream and downstream of a controlled large bifurcation—The Mississippi-Atchafalaya River diversion. *Hydrol. Process.* **2020**, *34*, 2864–2877. [[CrossRef](#)]
6. Xu, W.; Cheng, H.Q.; Zheng, S.W.; Jiang, Y.H.; Zhou, Q.P.; Yang, G.Q.; Yan, H.Z. Riverbed deformation and its response to human intervention on the lower reaches of the Yangtze River. *River Res. Appl.* **2022**, *38*, 222–234.
7. Tejedor, A.; Longjas, A.; Zaliapin, I.; Fofoula-Georgiou, E. Delta channel networks: 1. A graph-theoretic approach for studying connectivity and steady state transport on deltaic surfaces. *Water Resour. Res.* **2015**, *51*, 3998–4018. [[CrossRef](#)]
8. Nienhuis, J.H.; Ashton, A.D.; Giosan, L. Littoral steering of deltaic channels. *Earth Planet. Sci. Lett.* **2016**, *453*, 204–214. [[CrossRef](#)]
9. Syvitski, J.P.M.; Kettner, A.J.; Overeem, I.; Hutton, E.W.H.; Hannon, M.T.; Brakenridge, G.R.; Day, J.; Vorosmarty, C.; Saito, Y.; Giosan, L.; et al. Sinking deltas due to human activities. *Nat. Geosci.* **2009**, *2*, 681–686. [[CrossRef](#)]
10. Nittrouer, J.A.; Viparelli, E. Sand as a stable and sustainable resource for nourishing the Mississippi river delta. *Nat. Geosci.* **2014**, *7*, 350–354. [[CrossRef](#)]
11. Jiang, C.; Pan, S.Q.; Chen, S.L. Recent morphological changes of the Yellow River (Huanghe) submerged delta: Causes and environmental implications. *Geomorphology* **2017**, *293*, 93–107. [[CrossRef](#)]
12. Zheng, S.W.; Cheng, H.Q.; Lv, J.S.; Li, Z.J.; Zhang, L. Morphological evolution of estuarine channels influenced by multiple anthropogenic stresses: A case study of the north channel, Yangtze estuary, China. *Estuarine Coast. Shelf Sci.* **2020**, *249*, 107075. [[CrossRef](#)]
13. Dai, Z.J.; Fagherazzi, S.; Mei, X.F.; Gao, J. Decline in suspended sediment concentration delivered by the changjiang (Yangtze) River into the east China sea between 1956 and 2013. *Geomorphology* **2016**, *268*, 123–132. [[CrossRef](#)]
14. Shi, S.; Cheng, H.Q.; Xuan, X.N.; Hu, F.X.; Yuan, X.T.; Jiang, Y.H.; Zhou, Q.P. Fluctuations in the tidal limit of the Yangtze River estuary in the last decade. *Sci. China Earth Sci.* **2018**, *61*, 1136–1147. [[CrossRef](#)]
15. Kennish, M.J. Coastal saltmarsh systems in the U.S.: A review of anthropogenic impacts. *J. Coast. Res.* **2001**, *17*, 731–748.
16. Maloney, J.M.; Bentley, S.J.; Xu, K.; Obelcz, J.; Georgiou, I.Y.; Miner, M.D. Mississippi River subaqueous delta is entering a stage of retrogradation. *Mar. Geol.* **2018**, *400*, 12–23. [[CrossRef](#)]

17. Fu, Y.T.; Chen, S.L.; Ji, H.Y.; Fan, Y.S.; Li, P. The modern Yellow River Delta in transition: Causes and implications. *Mar. Geol.* **2021**, *436*, 10746. [[CrossRef](#)]
18. Wu, Z.; Milliman, J.D.; Zhao, D.; Cao, Z.; Zhou, C. Geomorphologic changes in the lower Pearl River Delta, 1850–2015, largely due to human activity. *Geomorphology* **2018**, *314*, 42–54. [[CrossRef](#)]
19. Ji, H.Y.; Chen, S.L.; Pan, S.Q.; Xu, C.L.; Jiang, C.; Pan, Y.S. Morphological variability of the active Yellow River mouth under the new regime of riverine delivery. *J. Hydrol.* **2018**, *564*, 329–341. [[CrossRef](#)]
20. Tang, M.; Xu, Y.J.; Xu, W.; Wang, B.; Cheng, H.Q. Three-decadal erosion and deposition of channel bed in the Lower Atchafalaya River, the largest tributary of the Mississippi River. *Geomorphology* **2018**, *380*, 107638. [[CrossRef](#)]
21. Yang, S.L.; Milliman, J.D.; Li, P.; Xu, K.H. 50,000 dams later: Erosion of the Yangtze River and its delta. *Glob. Planet. Chang.* **2011**, *75*, 14–20. [[CrossRef](#)]
22. Dai, Z.; Liu, J.T.; Wei, W.; Chen, J. Detection of the Three Gorges Dam influence on the Changjiang (Yangtze River) submerged delta. *Sci. Rep.* **2014**, *4*, 6600. [[CrossRef](#)] [[PubMed](#)]
23. Luan, H.L.; Ding, P.X.; Wang, Z.B.; Ge, J.Z. Process-based morphodynamic modeling of the Yangtze Estuary at a decadal timescale: Controls on estuarine evolution and future trends. *Geomorphology* **2017**, *290*, 347–364. [[CrossRef](#)]
24. Wang, B.; Xu, Y.J. Decadal-scale riverbed deformation and sand budget of the last 500 km of the Mississippi River: Insights into natural and river engineering effects on a large alluvial river. *J. Geophys. Res. Earth Surf.* **2018**, *123*, 874–890. [[CrossRef](#)]
25. Li, S.; Xu, Y.J.; Ni, M. Drastic changes in sediment, nutrients and major ions in the world largest Reservoir: Effects of damming and reservoir operation. *J. Clean. Prod.* **2021**, *318*, 128601. [[CrossRef](#)]
26. Xie, Q.; Yang, J.; Lundström, T.S. Sediment and morphological changes along Yangtze River’s 500 km between Datong and Xuliujing before and after Three Gorges Dam commissioning. *Sci. Rep.* **2021**, *11*, 13662. [[CrossRef](#)]
27. Wu, S.H.; Cheng, H.Q.; Xu, Y.J.; Li, J.F.; Zheng, S.W. Decadal changes in bathymetry of the Yangtze River Estuary: Human impacts and potential saltwater intrusion. *Estuar. Coast. Shelf Sci.* **2016**, *182*, 158–169. [[CrossRef](#)]
28. Zhou, X.Y.; Dai, Z.J.; Mei, X.F. The multi-decadal morphodynamic changes of the mouth bar in a mixed fluvial-tidal estuarine channel. *Mar. Geol.* **2020**, *429*, 106311. [[CrossRef](#)]
29. Zhu, B.Y.; Li, Y.T.; Yue, Y.; Yang, Y.P.; Liang, E.H.; Zhang, C.; Borthwick, A.G.L. Alternate erosion and deposition in the Yangtze Estuary and the future change. *J. Geogr. Sci.* **2020**, *30*, 145–163. [[CrossRef](#)]
30. Yang, S.L.; Zhang, J.; Dai, S.B.; Li, M.; Xu, X.J. Effect of deposition and erosion within the main river channel and large lakes on sediment delivery to the estuary of the Yangtze River. *J. Geophys. Res. Earth Surf.* **2007**, *112*, F02005. [[CrossRef](#)]
31. Chen, J.Y.; Yun, C.X.; Xu, H.G.; Dong, Y.F. The developmental model of the Chang Jiang River estuary during last 2000 years. *Acta Oceanol. Sin.* **1979**, *4*, 103–111. (In Chinese)
32. Cheng, H.Q.; Kostaschuk, R.; Shi, Z. Tidal currents, bed sediments, and bedforms at the South Branch and the South Channel of the Changjiang (Yangtze) estuary, China: Implications for the ripple-dune transition. *Estuaries* **2004**, *27*, 861. [[CrossRef](#)]
33. Wu, S.H.; Cheng, H.Q.; Xu, Y.J.; Li, J.F.; Zheng, S.W.; Xu, W. Riverbed micromorphology of the Yangtze River Estuary, China. *Water* **2016**, *8*, 190. [[CrossRef](#)]
34. McKean, J.; Nagel, D.; Tonina, D.; Bailey, P.; Wright, C.W.; Bohn, C.; Nayegandhi, A. Remote Sensing of Channels and Riparian Zones with a Narrow-Beam Aquatic-Terrestrial LIDAR. *Remote Sens.* **2009**, *1*, 1065–1096. [[CrossRef](#)]
35. Wheaton, J.M.; Brasington, J.; Darby, S.E.; Sear, D.A. Accounting for uncertainty in DEMs from repeat topographic surveys: Improved sediment budgets. *Earth Surf. Process. Landf.* **2010**, *35*, 136–156. [[CrossRef](#)]
36. Van Rijn, L.C. Sediment transport, part III: Bed forms and alluvial roughness. *J. Hydraul. Eng.* **1984**, *110*, 1733–1754. [[CrossRef](#)]
37. Li, J.H.; Jiang, E.H.; Zhang, B.M.; Zhang, Y. Stochastic analysis of threshold velocity of sediment particles. *J. Sediment Res.* **2012**, *3*, 15–20. (In Chinese)
38. Shields, A. *Application of Similarity Principles and Turbulence Research to Bed-Load Movement*; Ott, W.P.; van Uchelen, J.C., Translators; Hydrodyn. Lab. Publ. 167, W.M. Keck Lab. of Hydraul. And Water Resour; California Institute of Technology: Pasadena, CA, USA, 1936.
39. James, C.S. Prediction of entrainment conditions for nonuniform, noncohesive sediments. *J. Hydraul. Res.* **1990**, *28*, 25–40. [[CrossRef](#)]
40. Zhang, R.J. *Fluvial Sediment Dynamics*; Water Conservancy and Hydropower Press: Beijing, China, 1998.
41. Guo, X.J.; Cheng, H.Q.; Mo, R.Y.; Yang, Z.Y. Statistical characteristics and transport law of sand waves in the Yangtze Estuary. *Acta Oceanol. Sin.* **2015**, *37*, 148–158.
42. Wengrove, M.E.; Foster, D.L.; Lippmann, T.C.; de Schipper, M.A.; Calantoni, J. Observations of bedform migration and bedload sediment transport in combined wave-current flows. *J. Geophys. Res. Ocean.* **2019**, *124*, 4572–4590. [[CrossRef](#)]
43. Meyer-Peter, E.; Muller, R. Formulas for bed-load Transport. IAHSR 2nd Meeting. 1948, Volume 6, pp. 39–64. Available online: <https://repository.tudelft.nl/islandora/object/uuid:4fda9b61-be28-4703-ab06-43cdc2a21bd7?> (accessed on 1 January 2022).
44. Einstein, H.A. *The Bed Load Function for Sediment Transportation in Open Channel Flows*; Technical Bulletin 156389; United States Department of Agriculture, Economic Research Service: Washington, DC, USA, 1950.
45. Ackers, P.; White, W.R. Sediment transport new approach and analysis. *J. Hydraul. Div.* **1975**, *101*, 621–625. [[CrossRef](#)]
46. Mei, X.F.; Dai, Z.J.; Wei, W.; Li, W.H.; Wang, J.; Sheng, H. Secular bathymetric variations of the north channel in the changjiang (Yangtze) estuary, China, 1880–2013: Causes and effects. *Geomorphology* **2018**, *303*, 30–40. [[CrossRef](#)]

47. Zheng, S.W.; Cheng, H.Q.; Shi, S.Y.; Xu, W.; Zhou, Q.P.; Jiang, Y.H.; Zhou, F.N.; Cao, M.X. Impact of anthropogenic drivers on subaqueous topographical change in the Datong to Xuliujing reach of the Yangtze River. *Sci. China Earth Sci.* **2018**, *61*, 940–950. [[CrossRef](#)]
48. Guo, L.C.; Su, N.; Townend, I.; Wang, Z.B.; Zhu, C.Y.; Wang, X.Y.; Zhang, Y.N.; He, Q. From the headwater to the delta: A synthesis of the basin-scale sediment load regime in the Changjiang River. *Earth-Sci. Rev.* **2019**, *197*, 102900. [[CrossRef](#)]
49. Li, Y.M.; Zhang, G.A.; You, B.W.; Li, Z.H. Recent sediment characteristics and their impact factors in the Yangtze Estuary riverbed. *Acta Geogr.* **2019**, *74*, 178–190. (In Chinese)
50. Saucier, R.T. *Geomorphology and Quaternary Geologic History of the Lower Mississippi Valley*; U.S. Army Engineer Waterways Experiment Station: Vicksburg, MS, USA, 1994.
51. Cheng, H.Q.; Chen, J.Y.; Chen, Z.J.; Ruan, R.L.; Xu, G.Q.; Zeng, G.; Zhu, J.R.; Dai, Z.J.; Chen, X.Y.; Gu, S.H.; et al. Mapping sea level rise behavior in an estuarine delta system: A case study along the Shanghai coast. *Engineering* **2018**, *4*, 156–163. [[CrossRef](#)]
52. Ollive, E.A.; Edmonds, D.A.; Shaw, J.B. Influence of floods, tides, and vegetation on sediment retention in Wax Lake Delta, Louisiana, USA. *J. Geophys. Res. Earth Surf.* **2020**, *125*, e2019JF005316.
53. Gugliotta, M.; Saito, Y. Matching trends in channel width, sinuosity, and depth along the fluvial to marine transition zone of tide-dominated river deltas: The need for revision of depositional and hydraulic models. *Earth Sci. Rev.* **2019**, *191*, 93–113. [[CrossRef](#)]
54. Luan, H.L.; Ding, P.X.; Wang, Z.B.; Yang, S.L.; Lu, J.Y. Morphodynamic impacts of large-scale engineering projects in the Yangtze River delta. *Coast. Eng.* **2018**, *141*, 1–11. [[CrossRef](#)]
55. Sun, Y.; Li, B.; Yan, X.X.; Li, Y. Effect of north-south channel bifurcation control engineering on the north channel of Yangtze estuary. *J. Sediment Res.* **2018**, *43*, 33–38. (In Chinese)
56. Yang, T.; Tao, J.F.; Zhang, C.K.; Liu, G.P. Analysis on annual variation of diversion ratio of flow and sediment in Yangtze River Estuary after regulation project. *Yangtze River* **2012**, *43*, 84–88. (In Chinese)
57. Chen, D.; Dai, Z.J.; Xu, R.; Li, D.J.; Mei, X.F. Impacts of anthropogenic activities on the Changjiang (Yangtze) estuarine ecosystem (1998–2012). *Acta Oceanol.* **2015**, *34*, 86–93. [[CrossRef](#)]
58. Jiang, C.J.; Li, J.F.; de Swart, H.E. Effects of navigational works on morphological changes in the bar area of the Yangtze River estuary. *Geomorphology* **2012**, *139*, 205–219. [[CrossRef](#)]
59. Li, M.T.; Cheng, H.Q.; Zhou, F.N.; Wu, J.W.; Li, B.C. The effect to Sand Digging to bed from stability of the South Channel in the Changjiang River Mouth. *Hydrogr. Surv. Charting* **2011**, *31*, 54–57. (In Chinese)
60. Xia, J.; Zhang, Y.; Xiong, L.; He, S.; Wang, L.; Yu, Z. Opportunities and challenges of the sponge city construction related to urban water issues in China. *Sci. China Earth Sci.* **2017**, *60*, 652–658. [[CrossRef](#)]
61. Knaapen, M.A.F.; van Bergen Henegouw, C.N.; Hu, Y.Y. Quantifying bedform migration using multi-beam sonar. *Geo-Mar. Lett.* **2005**, *25*, 306–314. [[CrossRef](#)]
62. Hu, H.; Wei, T.Y.; Yang, Z.Y.; Hackney, C.R.; Parsons, D.R. Low-angle dunes in the changjiang (yangtze) estuary: Flow and sediment dynamics under tidal influence. *Estuar. Coast. Shelf Sci.* **2018**, *205*, 110–122. [[CrossRef](#)]
63. Zheng, S.W.; Cheng, H.Q.; Wu, S.H. Discovery and implications of catenary-bead subaqueous dunes. *Sci. China Earth Sci.* **2016**, *46*, 18–26. [[CrossRef](#)]
64. Wang, W.W.; Fan, F.X.; Li, C.G.; Yan, J. Activity of submarine sandwaves and seafloor erosion and deposition in the sea area to the southwest of Hainan Island. *Mar. Geol. Quat. Geol. Geol.* **2007**, *27*, 23–28. (In Chinese)
65. Paarlberg, A.J.; Dohmen-Janssen, C.M.; Hulscher, S.J.M.H.; Termes, P.; Schielen, R. Modelling the effect of time-dependent river dune evolution on bed roughness and stage. *Earth Surf. Process. Landf.* **2010**, *35*, 1854–1866. [[CrossRef](#)]
66. Wu, S.H.; Xu, Y.J.; Wang, B.; Cheng, H.Q. Riverbed dune morphology of the Lowermost Mississippi River—Implications of leeside slope, flow resistance and bedload transport in a large alluvial river. *Geomorphology* **2021**, *385*, 107733. [[CrossRef](#)]
67. Wu, J.X.; Wang, Y.H.; Cheng, H.Q. Bedforms and bed material transport pathways in the Changjiang (Yangtze) Estuary. *Geomorphology* **2009**, *104*, 175–184. [[CrossRef](#)]
68. Zheng, S.W.; Cheng, H.Q.; Wu, S.H.; Shi, S.Y.; Xu, W.; Zhou, Q.P.; Jiang, Y.H. Morphology and mechanism of the very large dunes in the tidal reach of the Yangtze River, China. *Cont. Shelf Res.* **2017**, *139*, 54–61. [[CrossRef](#)]
69. Unsworth, C.A.; Nicholas, A.P.; Ashworth, P.J.; Best, J.L.; Lane, S.N.; Parsons, D.R.; Sambrook Smith, G.H.; Simpson, C.J.; Strick, R.J.P. Influence of dunes on channel-scale flow and sediment transport in a sand bed braided river. *J. Geophys. Res. Earth Surf.* **2020**, *125*, e2020JF005571. [[CrossRef](#)]
70. Zhan, Y.Z.; Yu, M.H.; Deng, J.Y.; Lu, J.; Huang, L.W. Research on variation law of wave height based on current in tension. *J. Wuhan Univ. (Eng. Sci.)* **2006**, *4*, 10–13. (In Chinese)
71. Cheng, H.Q.; Li, M.T.; Zhou, T.Y.; Xue, Y.Z. High-resolution micro-topography movement in the Changjiang Estuary. *China Ocean Eng.* **2002**, *20*, 91–95. (In Chinese)
72. Southard, J.B.; Boguchwal, A.L. Bed configurations in steady unidirectional water flows; Part 2. Synthesis of flume data. *J. Sediment Res.* **1990**, *60*, 658. [[CrossRef](#)]
73. Luan, H.L.; Ding, P.X.; Wang, Z.B.; Ge, J.Z.; Yang, S.L. Decadal morphological evolution of the Yangtze Estuary in response to river input changes and estuarine engineering projects. *Geomorphology* **2016**, *265*, 12–23. [[CrossRef](#)]
74. Zheng, S.; Han, S.; Tan, G.; Xia, J.; Wu, B.; Wang, K.; Edmonds, D.A. Morphological adjustment of the qingshuigou channel on the yellow river delta and factors controlling its avulsion. *Catena* **2018**, *166*, 44–55. [[CrossRef](#)]

75. Anthony, E.J.; Brunier, G.; Besset, M.; Goichot, M.; Dussouillez, P.; Nguyen, V.L. Linking rapid erosion of the Mekong River delta to human activities. *Sci. Rep.* **2015**, *5*, 14745. [[CrossRef](#)]
76. Tang, M.; Xu, Y.J.; Wang, B.; Xu, W.; Cheng, H.; Tsai, F.T.-C. Artificial bifurcation effect on downstream channel dynamics of a large lowland river, the Atchafalaya. *Earth Surf. Process. Landf.* **2022**, *47*, 540–552. [[CrossRef](#)]
77. Törnqvist, T.E.; Bridge, J.S. Spatial variation of overbank aggradation rate and its influence on avulsion frequency. *Sedimentology* **2002**, *49*, 891–905. [[CrossRef](#)]
78. Syvitski, J.P.M.; Saito, Y. Morphodynamics of deltas under the influence of humans. *Glob. Planet. Chang.* **2007**, *57*, 261–282. [[CrossRef](#)]